

GW170817 and GW190425 as Hybrid Stars of Dark and Nuclear Matters

Kilar Zhang, Guo-Zhang Huang, and Feng-Li Lin¹

Department of Physics, National Taiwan Normal University, Taipei 11677, Taiwan

E-mail: kilar.zhang@gmail.com, 60641027s@ntnu.edu.tw, fengli.lin@gmail.com

Abstract. We propose three scenarios for compact hybrid stars consisting of nuclear and dark matters to interpret the LIGO/Virgo events GW170817 and GW190425. We use two equations of state (EoSs) for the nuclear matter in the hybrid stars, one is the SLy4 and the other is the one extracted from holographic quantum chromodynamics. On the other hand, for the dark matter we adopt the EoS extracted from the massive boson with quartic self-coupling, which is simple and capable of yielding both reasonable halo density and compact stars. We study the mass-radius and tidal Love number-mass relations for these compact hybrid stars, and find that they can well explain GW170817 and GW190425. Some of the hybrid stars can have compact neutron or mixed cores around 10km while possessing thick dark matter shells, which can then explain the astrophysical observations of neutron stars with compact photon radius and mass higher than 2 solar masses. Reversely, we also infer the dark matter model from the parameter estimation of GW190425. Our scenarios of compact hybrid stars can be further tested by the coming LIGO/Virgo O3 events.

¹Corresponding author.

Contents

1	Introduction	1
2	Model of equation of state for dark and nuclear matters	2
3	Tolman-Oppenheimer-Volkoff configuration and tidal Love number	6
4	M-R and Λ-M relations	7
4.1	For Scenario I and II:	7
4.2	For Scenario III:	10
5	Fitting of GW170817 and GW 190425	14
6	Parameter estimation for EoS of dark matter	15
7	Conclusion	17
A	Unify TOV equations and Tidal force for multi-component cases	19
A.1	Junction condition between core and crust	20

1 Introduction

Dark matter, though prevails over the universe and consists of about 3-quarter of matter content, reveals little evidence in the direct search in the past three decades [1–4]. The main difficulty of direct search is due to its rare interactions with the visible sector and thus the lack of the associated electromagnetic signals. On the other hand, everything gravitates. If dark matter can form the compact binary coalescences (CBC), one can detect the associated gravitational waves (GW) to infer its equation of state (EoS) and the corresponding microscopic theory of dark matter [5–7]. This can be thought as an alternative direct search through the relation between gravitational astronomy, microscopic and macroscopic physics of dark matter. There are some issues for the conventional models such as weakly interacting massive particles (WIMP) [8] to explain some of the observed properties of dark matter halos, such as the smooth core profile or the missing satellites, this then motivates to introduce the self-interacting dark matter (SIDM) to resolve these issues [9–12]. Moreover, if the dark matter is bosonic, the self-interaction will help to form compact stars of a few solar masses [13–16], which can further form binary hybrid stars (BHS) and yield GW from their CBC.

Given the possibilities of compact dark stars, one can further speculate the existence of compact hybrid stars made of dark and nuclear matters. This is the analogue to the dark halos made of dark and visible matters [17] but in a much smaller scale. There are three scenarios of compact hybrid stars as shown in Fig. 1, which depend on how dark and nuclear matters interact, and also on the accretion mechanism. The first scenario is to have the stars with neutron core and dark matter shell, the second is the ones with dark matter core and neutron shell. For both scenarios we assume there is interaction between dark and nuclear matters, or spontaneous symmetry breaking to form the domain wall separating the core and shell. Otherwise, it will lead to the third scenario for which the dark and nuclear matters are mixed inside the core but with only one component in the shell. These hybrid stars can be

seen as the cousins of neutron stars with the new parameter r_W characterizing the radius of the the inner core. Here, we simply assume the existence of these hybrid stars and leave their formation mechanism for future studies.¹

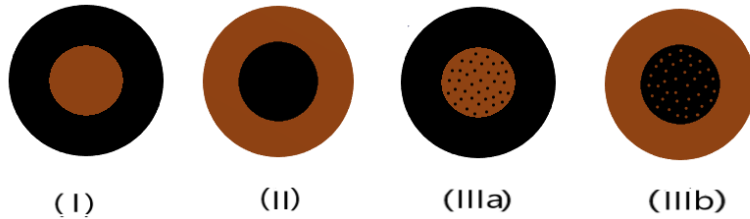


Figure 1. Three scenarios of hybrid stars. Black color denotes dark matter and brown color denotes nuclear matter. In the first scenario the star consists of a pure nuclear matter core and a pure dark matter shell, and consists of a pure dark matter core and a pure nuclear matter shell in the second scenario. In the third scenarios, we have a mixed core and either a pure dark matter shell (IIIa) or a pure nuclear matter one (IIIb). They can form the systems of binary hybrid stars (BHS).

Despite the speculated hybrid stars, it is hard to detect them due to either lack of electromagnetic signals or not enough telling from the neutron stars. However, these hybrid stars will have different mass-radius relation and the tidal deformability which can be encoded in the GW emitted from the coalescences of BHS. Thus, we may test the above three scenarios for BHS via GW events discovered by LIGO/Virgo. Currently, there are two observed events usually identified as binary neutron stars, namely, GW170817 [25, 26] and GW190425 [27]. The key feature of both events is their low tidal Love numbers (TLNs). Moreover, the total mass and the associated component masses of GW190425 seem larger than the ones expected for the neutron stars, in comparison to GW170817. These features can call for the alternative explanation such as the one provided by hybrid stars. Reversely, we can constrain the associated dark matter model by analyzing the hydrodynamical properties of the hybrid stars from the GW data.

The organization of the paper is as follows: In section 2 we introduce the EoSs for the models used for dark and nuclear matters; Section 3 shows TOV configurations and how to calculate tidal Love number; Section 4 illustrates M - R and Λ - M relations from our numerical results; In section 5 we fit GW170817 and GW 190425 using our model; Section 6 describes parameter estimation for EoS of dark matter; Section 7 is the conclusion and in the appendix we offer more details on TOV and tidal equations.

2 Model of equation of state for dark and nuclear matters

In this paper, we show that both GW170817 and GW190425 can be easily explained by a simple toy model of hybrid stars based on the above three scenarios. We do not aim to pin down the models for nuclear and dark matters, but to demonstrate the viability of the hybrid star scenarios. Thus, we consider a simple model of nuclear and dark matters. We adopt the SIDM of a bosonic scalar field ϕ with potential $m^2\phi^2 + \frac{\lambda}{4}\phi^4$. Moreover, we consider the model

¹The capture rate of dark matter by neutron star is too small to form sizable share in the hybrid stars due to the weak interaction between dark matter and baryons [18, 19]. However, there are proposals to dramatically increase the cross-section by forming the nuggets [20–23] so that the capture rate could be accelerated. Another possibility for quickly accumulating dark matters is through the Bondi accretion [24].

in the regime $\lambda M_{\text{plank}}^2/m^2 \gg 1$ so that it can be equivalently described by a hydrodynamical perfect fluid with EoS given by [13]

$$\rho/\rho_\odot = 3 (p/p_\odot) + \mathcal{B} (p/p_\odot)^{1/2} \quad (2.1)$$

where $\mathcal{B} \sim \frac{0.08}{\sqrt{\lambda}} (\frac{m}{\text{GeV}})^2$ is a free parameter². In this paper we will adopt the astrophysical units:

$$r_\odot = G_N M_\odot / c^2, \quad \rho_\odot = M_\odot / r_\odot^3, \quad p_\odot = c^2 \rho_\odot,$$

for the (half) Schwarzschild radius of the Sun, the corresponding energy density and pressure, respectively. Note that M_\odot denotes the solar mass, and G_N the Newton constant.

There are many bosonic dark matter model candidates, some of which predict light dark matter particle such as axion [28]. However, if the dark matter is too light, it is not easy to form compact stars of a few solar masses [29] but the dark cloud around the compact stars or black holes [30]. Thus, for our purpose of searching for the compact stars around several solar masses, it is more natural to choose massive dark matter with mass around MeV to GeV. Moreover, it shows that the free massive dark matter may not be able to yield smooth dark halo profile but needs to introduce some self-interaction to fix the issue [9–12]. The simplest model from effective theory point of view is the SIDM with quartic coupling as introduced above. For this SIDM to explain the smooth density profile of dark halos, it will impose the constraint on the cross section of self-scattering, which is translated into a tiny window for λ [12]:

$$30 (\frac{m}{\text{GeV}})^{3/2} < \lambda < 90 (\frac{m}{\text{GeV}})^{3/2}. \quad (2.2)$$

Therefore, if we can pin down the parameter \mathcal{B} from the GW events, we can almost determine the parameters of SIDM.

As a first step, in this paper we only consider bosonic SIDM, however, the fermionic SIDM with Yukawa coupling constrained by the observed dark halo profile should be also viable for the formation of compact hybrid stars. For example, in [5, 6] the EoS for this kind of fermionic SIDM has been obtained and used to study the compact star configurations. One can follow the same procedure of this paper to consider the compact hybrid stars with fermionic SIDM.

As for the nuclear matter, we consider two model EoSs. One is the SLy4 [34, 35] used extensively in gravitational wave data analysis [25–27]. The other one is obtained in [36] from a well-motivated holographic quantum chromodynamics model, i.e., Sakai-Sugimoto model [37–39], and it takes the form

$$\rho/\rho_\odot = 2.629 \mathcal{A}^{-0.192} (p/p_\odot)^{1.192} + 0.131 \mathcal{A}^{0.544} (p/p_\odot)^{0.456}. \quad (2.3)$$

We denote this EoS as ‘‘Holo’’, the short-handed notation for holography. The advantage of Holo EoS is its simplicity with just one free dimensionless parameter \mathcal{A} . It has been used to well explain GW170817 [36] with $\mathcal{A} \sim 0.3$. However, this EoS is only good for the core of the neutron star, where nuclear matter density is around several times of the nuclear saturation density (n_s). Below n_s as in the neutron star crust and outer core, it is better to switch to the one in SLy4. In Fig. 2 we compare the EoSs of SLy4, Holo, and the combined one of both,

² This EoS is slightly below the sound barrier and takes the same form as the conjectured EoS of quark matter in the deep core of neutron star [31, 32]. The coincidence is due to the ϕ^4 potential and the nearly massless nature of quarks in the high chemical potential limit. If one consider higher ϕ^n with $n > 4$, the resultant EoS can break sound barrier [33].

denoted as Combo, i.e., we adopt Holo when the energy density is above the lower intersection point of SLy4 and Holo (see Fig. 2), and then switch to SLy4 below that point. The nuclear matter density is about $0.3n_s$ at the lower intersection point³, which is a reasonable nuclear matter density for the intersection between core and crust of a neutron star. Moreover, in Fig. 3 and Fig. 4 we compare the corresponding mass-radius relations and mass-TLN relations, respectively.

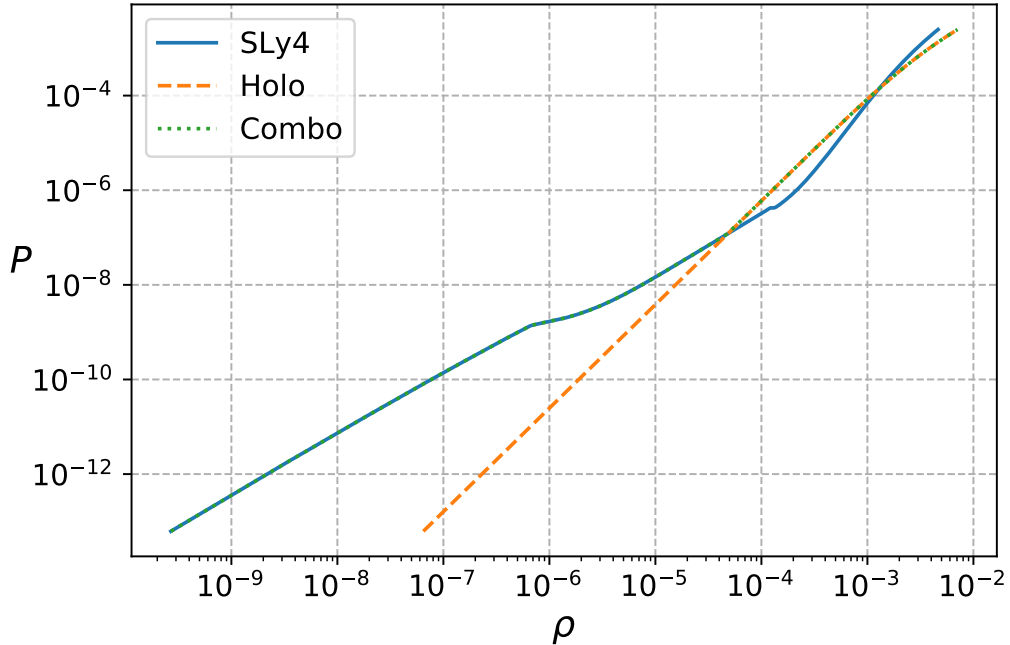


Figure 2. Comparison of three EoSs for nuclear matter: SLy4 (solid blue), Holo (dashed orange) and Combo (dotted green). Note that for Holo we set $\mathcal{A} = 0.305$ in this plot so that it can fit the parameter estimation (PE) of GW170817 and GW190425 [25–27, 36], and for SLy4 we choose the parameters so that it can also fit the PE of GW170817 and GW190425 but at the same time can yield configurations with mass larger than $2M_\odot$. We will use the same parameters for SLy4 through out the paper.

From Fig. 3 we see that Holo EoS cannot yield the neutron star configuration with the maximal mass greater than $2M_\odot$, which has been observed astronomically [40]. However, this Holo EoS can fit to the observational PE results of GW170817 [36] and GW190425⁴. Despite of that, as we will see below this Holo EoS can yield the hybrid stars of the first scenario with mass about $2M_\odot$ and 10 km nuclear core but with 20km dark matter shell. Observationally, this hybrid star should just have a visible 10km size to the X-ray observation [43–45] because the dark matter shell is invisible. This introduces the new degeneracy for the physical interpretation of the massive compact stars.

Finally, as shown in Fig. 4 the mass-TLN relations for Holo and Combo are almost the same. Besides, their mass-radius relations also match well for mass larger than $1.7M_\odot$ as seen

³This can be estimated by the Eq. (22) of [36] with the help of relations (18)-(20) in that paper for $p \sim 10^{-6} p_\odot$.

⁴This is easy to see because the TLN shown in Fig. 4 is low enough for $1.7M_\odot$ to be compatible with the TLN of GW190425 by assuming the source to be two neutron stars of $1.7M_\odot$.

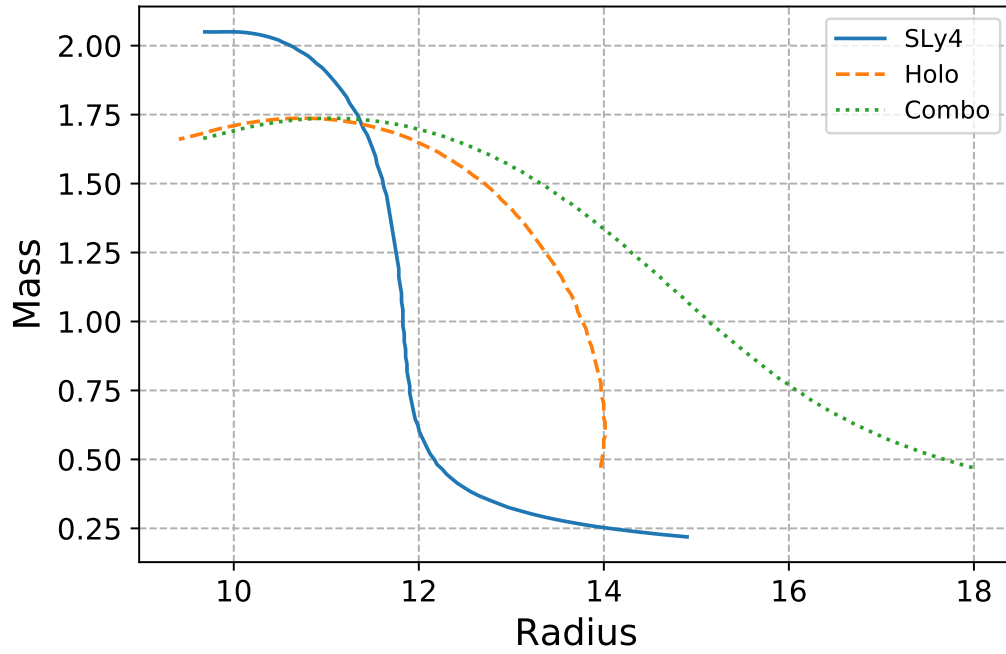


Figure 3. Comparison of Mass-Radius relations for the three EoSs given in Fig. 2: SLy4 (solid blue), Holo (dashed orange) and Combo (dotted green).

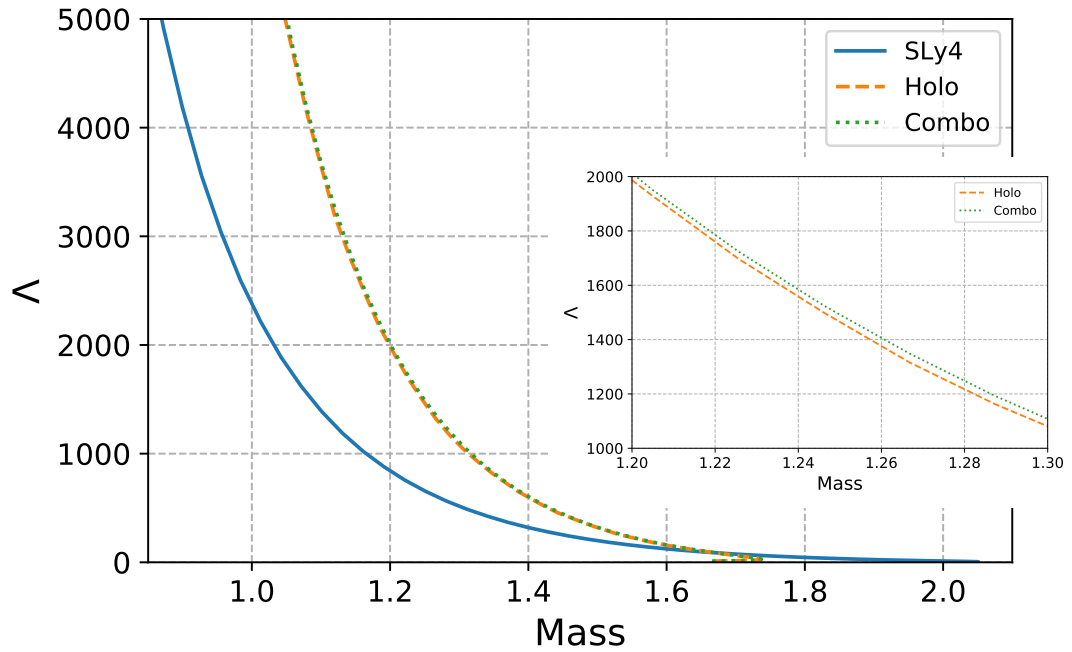


Figure 4. Comparison of Mass-TLN relations for the three EoSs given in Fig. 2: SLy4 (solid blue), Holo (dashed orange) and Combo (dotted green). The inset shows the minor difference between Holo and Combo.

from Fig. 3. Since we are concerning about the physical interpretation of GW events as the hybrid stars, for which the TLN is more relevant than radius, thus for simplicity we will just use Holo and SLy4 for the following discussions but not the Combo one.

3 Tolman-Oppenheimer-Volkoff configuration and tidal Love number

The GW of CBC encodes the component masses $M_{1,2}$, and also the TLNs $\Lambda_{1,2}$ in the following combined quantity

$$\tilde{\Lambda} = \frac{16}{13} \frac{(M_1 + 12M_2)M_1^4\Lambda_1 + (M_2 + 12M_1)M_2^4\Lambda_2}{(M_1 + M_2)^5}. \quad (3.1)$$

Note that $\tilde{\Lambda} = (\Lambda_1 + \Lambda_2)/2$ for $M_1 = M_2$. For each hybrid star scenario, we have three model parameters \mathcal{A} , \mathcal{B} and r_W . We shall connect the model parameters to the inferred quantities from observation data by the mass-radius and TLN-mass relations.

Given a set of $(\mathcal{A}, \mathcal{B}, r_W)$ we first obtain the mass-radius relation by solving the Tolman-Oppenheimer-Volkoff (TOV) equations⁵ using units $G = c = 1$:

$$p'_I = -(\rho_I + p_I)\phi', \quad m'_I = 4\pi r^2 \rho_I, \quad \phi' = \frac{m + 4\pi r^3 p}{r(r - 2m)}, \quad (3.2)$$

where $' := \frac{d}{dr}$, $I = D$ or N , the mass inside radius r is $m(r) = \sum_I m_I$, pressure $p = \sum_I p_I$, energy density $\rho = \sum_I \rho_I$ by summing the contributions from both dark matter ($I = D$) and nuclear matter ($I = N$), and the Newton potential $\phi := \frac{1}{2} \ln(-g_{tt})$ with g_{tt} the tt -component of the metric. The size R of the star is determined by $p(r = R) = 0$, and the mass of the star is given by $m(R)$. For the first scenario, we set $p_D = \rho_D = 0$ and use (2.3) to solve TOV equations for $r \leq r_W$. For $r \geq r_W$ we set $p_N = \rho_N = 0$ and set initial value of p_D at r_W equal to $p_N(r_W)$, then use (2.1) to solve the TOV equations until $r = R$. For the second scenario we do the same thing by swapping the roles of dark and nuclear matters. For the third scenario, we tune the initial values at $r = 0$ for both p_D and p_N and use both (2.1) and (2.3) to solve TOV. In this case r_W is determined by the first vanishing p_I , then we solve the TOV equations for $r > r_W$ until $r = R$ for the remaining nonvanishing p_I component.

A key difference between first two scenarios and the third one is the stability issues. For the first twos, we have just one initial-value parameter for solving TOV, i.e., either $p_D(0)$ or $p_N(0)$, but have both for the third one, thus the stability issue of the latte is more tricky due to possible saddle instability. As we will see, there are more massive stable configurations than the single fluid ones for the first two scenarios, but less in the third one.

After having solved the stable TOV configurations, we solve the linear perturbation around them to extract the TLN, Λ defined by

$$Q_{ab} = - (M/M_\odot)^5 \Lambda \mathcal{E}_{ab} \quad (3.3)$$

where Q_{ab} is the induced quadrupole moment, and \mathcal{E}_{ab} is the external gravitational tidal field strength. As shown in [46, 47], to obtain Λ , we first need to solve the following equation for $y(r) := rH'(r)/H(r)$ with $H(r)$ the linear perturbation of g_{tt} around a TOV configuration:

$$ry' + y^2 + P(r)y + r^2Q(r) = 0 \quad (3.4)$$

⁵See appendix A for more details.

with boundary condition $y(0) = 2$ and

$$P = (1 + 4\pi r^2(p - \rho))/(1 - 2m/r), \quad (3.5)$$

$$Q = 4\pi(5\rho + 9p + \sum_I \frac{\rho_I + p_I}{dp_I/d\rho_I} - \frac{6}{4\pi r^2})/(1 - 2m/r) - 4\phi'^2. \quad (3.6)$$

Moreover, due to the jump $\Delta\rho$ of ρ at $r = r_W$ for the first two scenarios, we need to impose the following junction condition on the jump Δy of y at $r = r_W$:

$$\Delta y = \Delta\rho/(p + m/4\pi r^3)|_{r=r_W}. \quad (3.7)$$

Once (3.4) is solved, the TLN Λ can be obtained through an algebraic expression of $y_R \equiv y(R)$ and the ‘‘compactness’’ $C = M/R$ given by [46, 47]

$$\Lambda = \frac{16}{15} (1 - 2C)^2 [2 + 2C(y_R - 1) - y_R] \times \left\{ 2C(6 - 3y_R + 3C(5y_R - 8)) + 4C^3 [13 - 11y_R + C(3y_R - 2) + 2C^2(1 + y_R)] + 3(1 - 2C)^2 [2 - y_R + 2C(y_R - 1)] \log(1 - 2C) \right\}^{-1}. \quad (3.8)$$

4 M - R and Λ - M relations

Based on the above we evaluate the M - R and Λ - M relations for the three hybrid star scenarios with dark matter EoS given by (2.1) and the nuclear matter EoS given by Holo of (2.3) and SLy4.

4.1 For Scenario I and II:

We first consider the case with the Holo EoS for nuclear matter. In Fig. 5 we show the M - R relations for the first two scenarios for $\mathcal{A} = 0.305$ and $\mathcal{B} = 0.035$ (with various r_W labelled as **aRN** for the first scenario, and as **aRD** for the second.) or $\mathcal{B} = 0.055$ (labelled by **bRN** and **bRD**), and in Fig. 6 we show the corresponding Λ - R relations. From the results we observe the followings. (i) The one labelled by **aRD**= 0 is the pure neutron stars which have been used to explain GW170817 in [36]. Now we see that the hybrid stars labelled by **aRD**= 8, i.e., 8km, can reach the maximum mass more than $2M_\odot$ but with $R \simeq 13$ km even though the pure neutron star **aRD**= 0 can only have maximum mass around $1.7M_\odot$. (ii) For the first scenario, we see that there is a jump around **aRN**= 10.2 or **bRN**= 9.5 (though the latter not shown explicitly in Fig. 5) beyond which the small-radius configurations become unstable (indicated by dash line in Fig. 5), this may imply some first order phase transition. On the other hand, above this critical **RN**, there are more compact hybrid stars which can be consistent with LIGO observation with small TLN as indicated in Fig. 6. (iii) The configuration with M larger than $3M_\odot$ are mainly composed by dark matters as seen from the ratio of r_W/R . Contrarily, the more compact hybrid stars of smaller R are mainly composed by nuclear matters. This is understandable as the Holo EoS (2.3) is stiffer than EoS (2.1). It then implies that the final state of the most binary hybrid stars’ mergers are unstable unless the initial stars are almost pure dark stars. Thus, if the component stars of GW190425 are the hybrid stars of these two scenarios, the final state will collapse into a black hole.

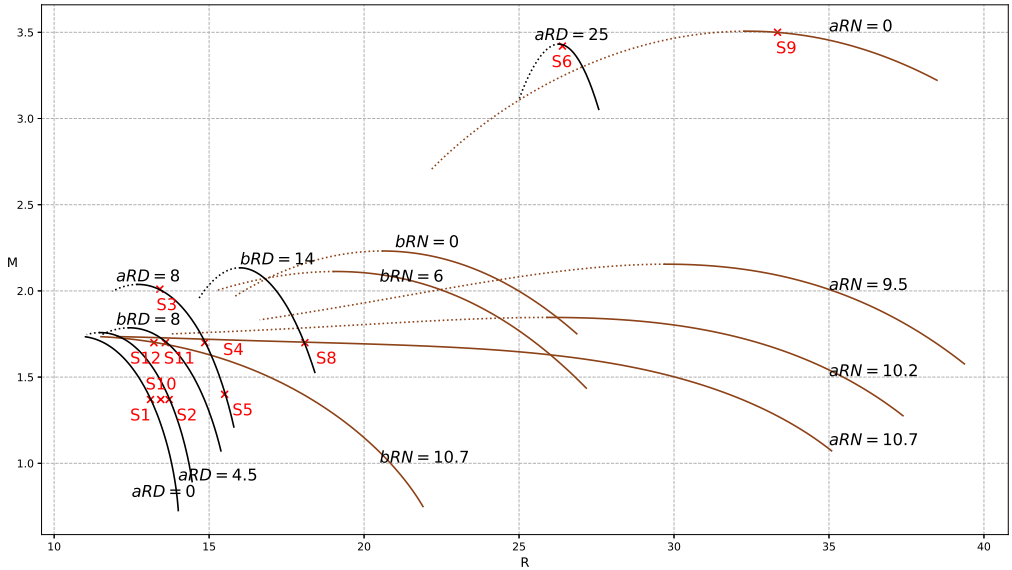


Figure 5. Mass-Radius relations for the hybrid stars of type (I) and (II) in Fig. 1, which are made of nuclear matter of Holo EoS with $\mathcal{A} = 0.305$ and dark matter of EoS (2.1) with $\mathcal{B} = 0.035$ or 0.055 . With $\mathcal{B} = 0.035$ these relations are labelled by $\mathbf{aRN} = r_W$ (brown) for the first scenario, by $\mathbf{aRD} = r_W$ (black) for the second. Similarly, with $\mathcal{B} = 0.055$ they are labelled by $\mathbf{bRN} = r_W$ (brown) and $\mathbf{bRD} = r_W$ (black)). For example, $\mathbf{aRD} = 8$ means the radius of dark core is 8km. The unstable configurations are indicated by the parts of dashed lines.

In comparison with Fig. 5 and 6 based on Holo EoS, we also obtain the hybrid star configurations by replacing the Holo EoS with the SLy4 one while keeping the same dark matter EoS as before. The M - R and Λ - R relations are shown in Fig. 7 and Fig. 8, respectively. The notations in these two figures such as \mathbf{aRN} etc. are the same as before, namely \mathbf{a} referring to EoS (2.1) with $\mathcal{B} = 0.035$, and \mathbf{b} to $\mathcal{B} = 0.055$. The main difference from the previous case is on the part of the sizable nuclear matter core by now having higher masses for the same radius. Especially, in this regime most of the maximal masses are now $2M_\odot$ or higher, in contrast to the previous Holo case with about $1.7 M_\odot$ with about the same size of TLN. This is expected as the nuclear matter EoS is now SLy4. Therefore, these hybrid stars can both fit to the GW170817 and the traditional astronomical observations. Moreover, we may also expect that the transition from nuclear matter dominance to the dark matter dominance will be also different. For example, as the dark matter core increases its size, the maximal mass goes down first as the boson EoS is less stiff, then go up as the allowed maximal mass of boson EoS is higher, and at the same time the total radius becomes larger. Otherwise, the other features are similar to the ones shown in Fig. 5 and 6, especially the points (ii) and (iii) in the discussions of previous paragraph.

In a short summary: in general, due to the additional component of matters, our hybrid stars can host a wider range of masses and TLNs than the pure neutron stars or dark stars. This will then be taken as the special feature to distinguish from the pure neutron and dark stars of a given EoS in the forthcoming GW observational data.

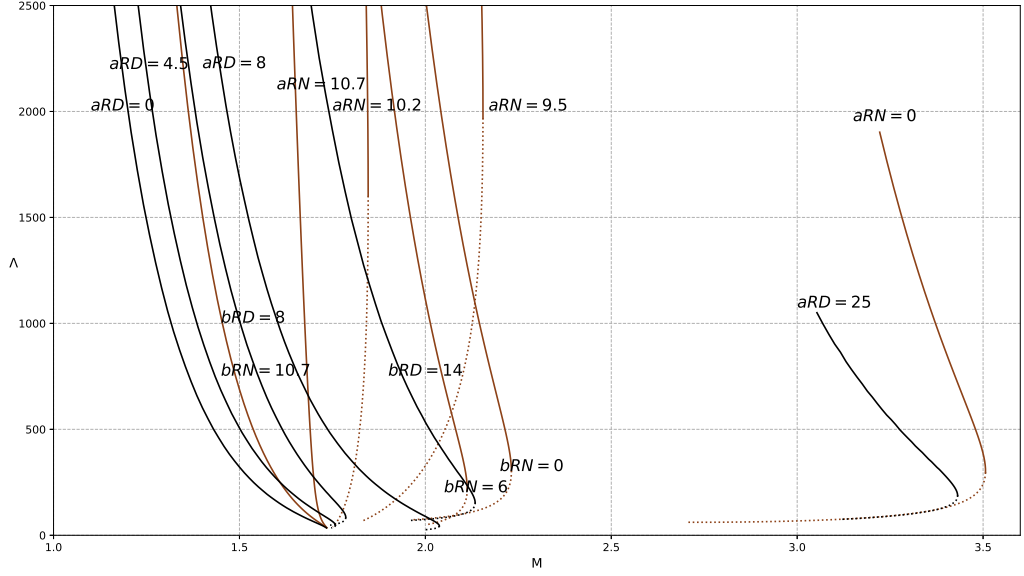


Figure 6. Corresponding TLN-Mass relations of Fig. 5. Similarly, the unstable configurations are indicated by the parts of dashed lines.

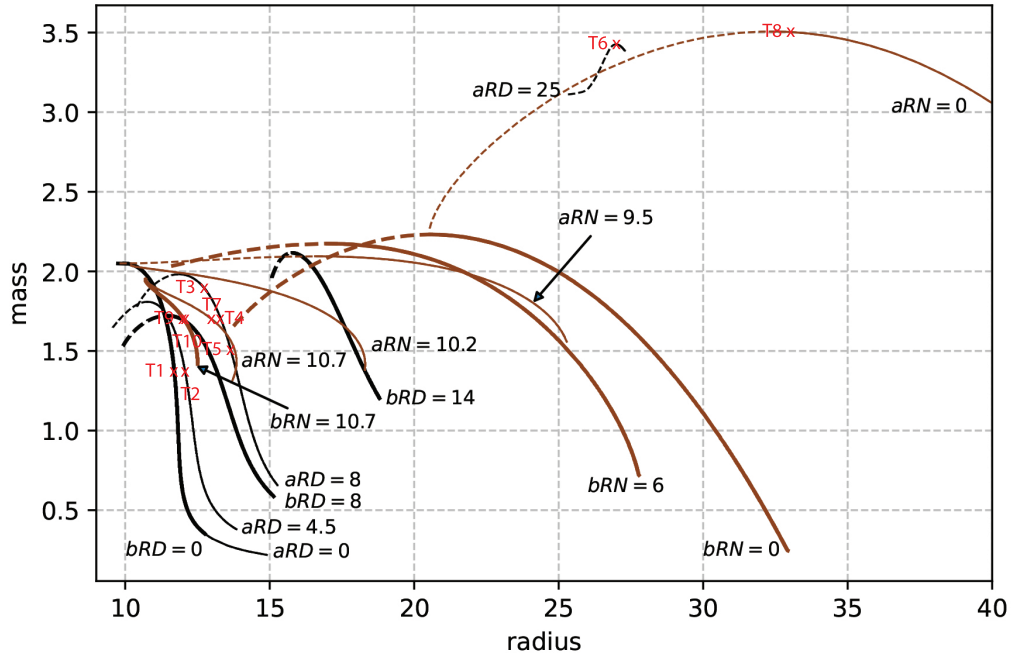


Figure 7. Mass-Radius relations for the hybrid stars of type (I) and (II) in Fig. 1, which are made of nuclear matter of SLy4 EoS and dark matter of EoS (2.1) with $\mathcal{B} = 0.035$ or 0.055 . The label conventions are the same as the ones in Fig. 5.

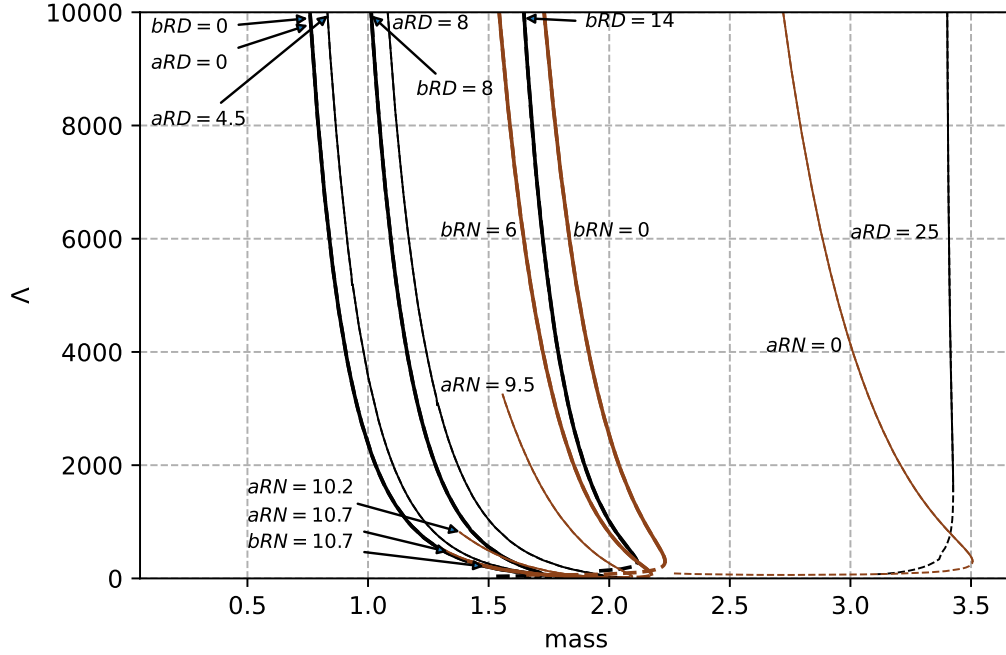


Figure 8. Corresponding TLN-Mass relations of Fig. 7. Similarly, the unstable configurations are indicated by the part of dashed lines.

4.2 For Scenario III:

Next, we show the M - R and Λ - M relations for the third scenario of hybrid stars, namely the mixed ones in the core, and the associated star configurations are denoted by **BMX** for $\mathcal{B} = 0.055$ of dark matter EoS and for either Holo EoS or SLy4 one of nuclear matter. In Fig. 9 we show the result for Holo EoS with $\mathcal{A} = 0.305$, and in Fig. 10 we show the results for SLy4.

Unlike the first two scenarios, there are saddle instabilities for the third scenario. Here we like to elaborate on the criterion for judging the stable regions. A simple way of determining the stable region is the so-called BTM (Bardeen-Thorne-Meltzer) criteria⁶ [41] as follows: We start with the stable configuration with very low core pressure, and trace along the M - R curve by increasing the core pressure. Then, when passing through an extremum on the M - R curve, we can have the following two situations: (1) If the M - R curve bends counterclockwise, a stable mode will become unstable; (2) Otherwise, one unstable mode become stable. By this way, we can determine which part on the M - R curve admits stable configurations.

However, in most of the cases we will not solve the M - R curve from the the very low core pressure, such as the case considered here. To determine the stability of the regime interested, we can assume the stability/instability of a certain part of the M - R curve, and then apply the BTM criteria reversely as follows,

Reverse BTM Stability Criteria: when passing through each extremum of the M - R curve in the direction of decreasing the core pressure,

1. if the M - R curve bends clockwise, one unstable mode becomes stable;

⁶This was shown in [41] to be equivalent to the stability analysis by solving the Sturm-Liouville eigenmodes of radial oscillation.

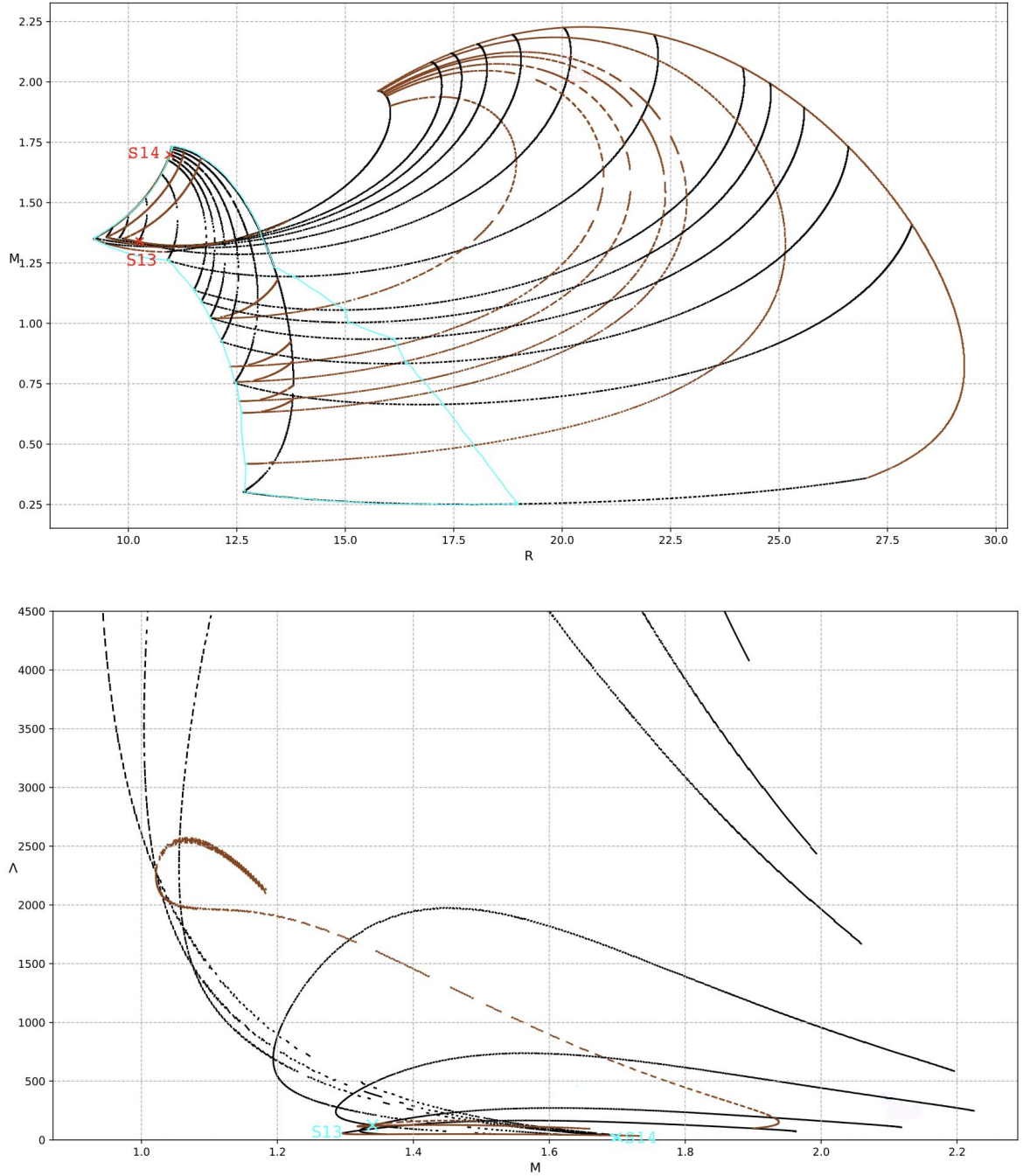


Figure 9. Mass-Radius (Up) and TLN-Mass (Down) relations and for the hybrid stars of type (IIIa) and (IIIb) in Fig. 1 for Holo EoS with $\mathcal{A} = 0.305$ and for dark matter EoS (2.1) with $\mathcal{B} = 0.055$ (labelled by **bMX** in the text and Table 1). The region of stable configurations is specified by the aqua-encircled area. Different black lines correspond to different core pressures of dark matter but varying the core pressures of the nuclear matter, and the brown lines are the other way around.

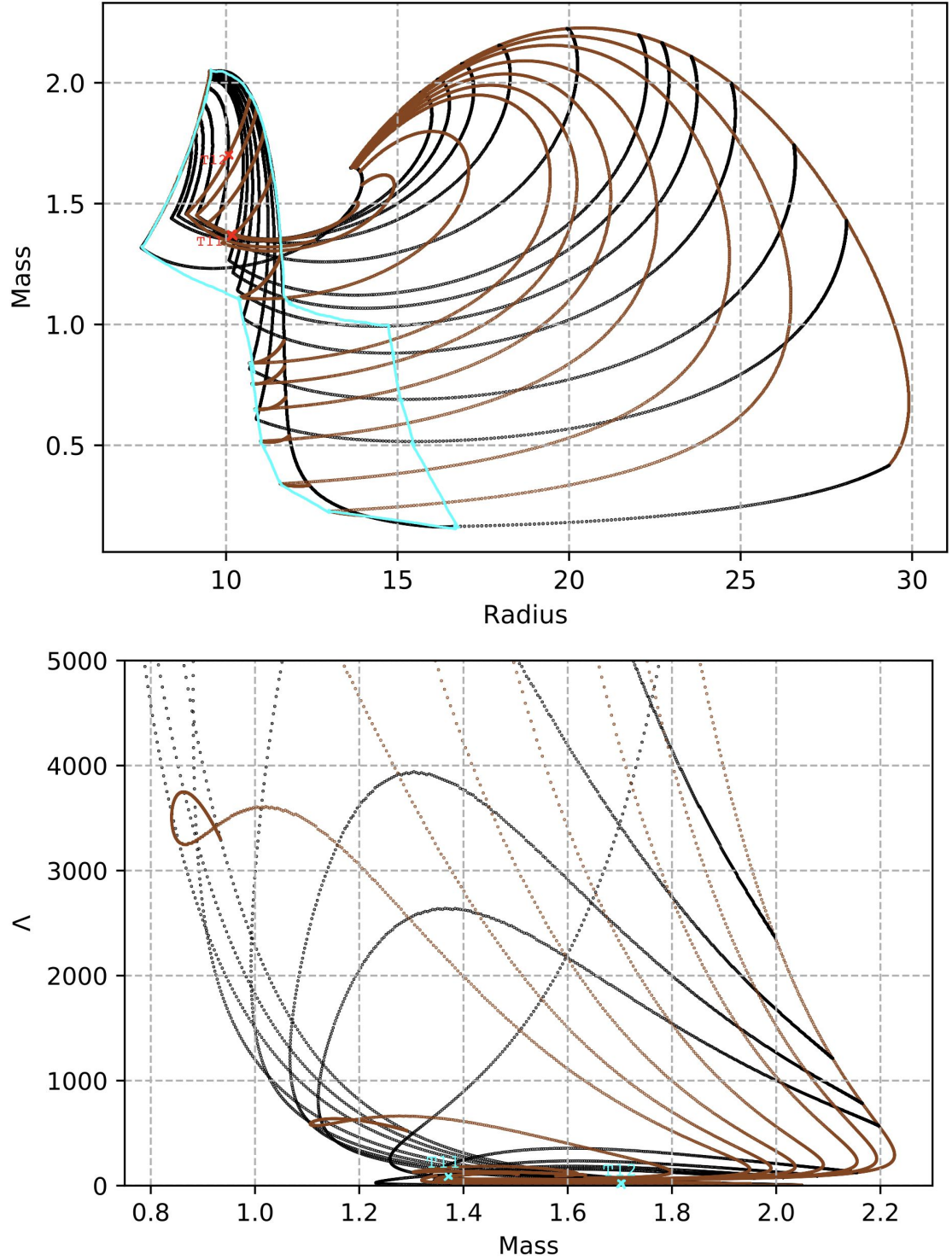


Figure 10. Mass-Radius (Up) and TLN-Mass (Down) relations and for the hybrid stars of type (IIIa) and (IIIb) in Fig. 1 for SLy4 EoS and for dark matter EoS with $\mathcal{B} = 0.055$. The region of stable configurations is specified by the aqua-encircled area. The line style is the same as in Fig. 9.

2. Otherwise, one stable mode becomes unstable.

After that, we can apply the BTM criteria on the same regime for consistency check to determine the stability/instability of the initial part. Some examples for the above practice are shown in Fig. 11 where the solid lines denote the stable regions, and the unstable parts the unstable ones. The arrows indicate the direction of increasing core pressure. Note that curves $O-A-B-C$ and $O'-A'-D'-B'-C'$ look quite similar but differ by the extremum D' . Thus, they have quite different stability/instability structures after applying the above (reverse) BTM criteria.

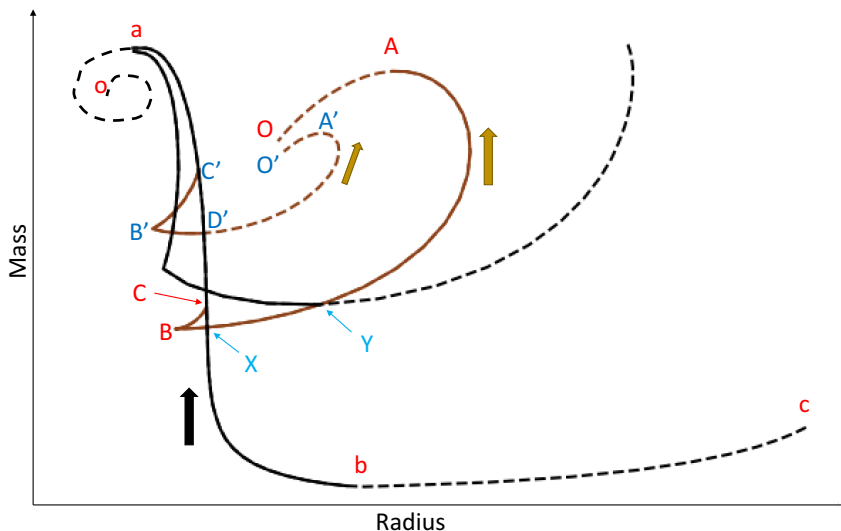


Figure 11. Some typical examples for the stability regimes of the $M-R$ curve of the third scenario hybrid stars. The black curves are NS-like and the brown curves are DM-like, which are defined in the main text. The block arrows indicate the directions of increasing of the core pressures. We use the (reverse) BTM criteria discussed in the main text to determine the stable/unstable regimes, which are indicated by solid/dotted parts. A caveat for the intersection point is as follows. Since the mass and radius depend on both the core pressures of nuclear and dark matters, some of the intersection points may be the faked ones and cannot be used to judge the saddle (in)stability. For examples, the intersection points C and Y are real ones, while the point X is a fake intersection point. For more details, see the main text.

Moreover, in the third scenario of hybrid stars, we have two orthogonal ways of changing the core pressures, and thus arrive at two sets of $M-R$ curves. One set called NS-like is to fix the core pressure of dark matter but change the one of the nuclear matter, and the other one called DM-like is the other way around. A typical example is shown in Fig. 11, where the black curves are NS-like and the brown curves are DM-like. We apply the above (reverse) BTM criteria to determine the stability/instability regime of each curve, then look for the regimes where both NS-like and DM-like curves admit stability. These regimes will then be identified as the stable hybrid stars of third scenario. However, there is one caveat. In Fig. 11 we see that one brown curve may intersect one black curve twice, for example, the C and X on the curve $O-A-B-C$. Since on the same black curve, the core pressure of the dark matter part is fixed, so one of them will be the fake intersection point. In this case, X is not the "real" intersection point since C is the starting point at which the core pressure of the dark

matter equal to the one on the black curve. Thus, the intersection point X will not be used to judge the saddle stability. Another subtle issue is if there is a change of stability around the sharp edge points such as B and B' at which a first order phase transition between from a nuclear crust to a dark crust may happen. In [42] it was shown that there is a stability change around such a point. However, due to fact that $B'-D'$ and $B-A$ are already stable, the $C'-D'$ and $C-B$ shall be stable no matter if we adopt the criterion of [42].

By applying the lessons learned from the typical examples in Fig. 11, we can roughly mark the stable regimes in both Fig. 9 for the Holo EoS and Fig. 10 for SLy4 one by the aqua-encircled areas. We see that the stable hybrid stars of the third scenario are limited to left part of the $M-R$ curves, which are more NS-like which can have the maximum masses comparable with the ones for pure neutron stars. However, there are no stable DM-like hybrid stars due to the saddle instability. Moreover, as in the first two scenarios, our hybrid stars can feature a wider range of masses and TLNs than the pure neutron stars of a given EoS.

5 Fitting of GW170817 and GW 190425

After discussing the general $M-R$ and $\Lambda-R$ relations for the three scenarios of compact hybrid stars, we now pick up some specific configurations as listed in Table 1 which can be identified as the component stars for the GW170817 and GW 190425. In Table 1 we have listed 26 hybrid stars labeled by the index Sn with $n=1\cdots 14$ and Tn with $n=1\cdots 12$. Most of them are indicated on Fig. 5, 7, 9 and 10. The types **aRD**, **aRN**, **bRD**, **bRN** and **bMX** are defined as before to indicate the different choices of core radius and \mathcal{B} , applying to both Holo EoS and the SLy4 EoS. The type **cRD** for S7 is a hybrid star of the second scenario with Holo EoS of $\mathcal{A} = 0.341$ and dark matter EoS of $\mathcal{B} = 0.055$, which is not shown in the above $M-R$ relation Figures. Especially, we list S6, S9, T6 and T8 to show that the typical high mass stars with mass larger than $3M_\odot$ are mainly the dark stars and cannot be the final states of the mergers of the low mass hybrid stars which are mainly composed of nuclear matter. Besides, most of the stars with masses lower than $2M_\odot$ have radii just 2 or 3km larger than the typical radii of neutron stars, say around 11km. Some of them such as S8, S12, T7 and T10 yet have 10.7km neutron cores to be consistent with the observed photon radius [43–45].

Note that for GW170817, the inferred total mass $M_1 + M_2 \simeq 2.73_{-0.01}^{+0.04} M_\odot$ with $M_1 \in (1.36, 1.60)M_\odot$, $M_2 \in (1.16, 1.36)M_\odot$ and $\tilde{\Lambda} = 300_{-230}^{+420}$ for low-spin prior. For simplicity, we consider the equal mass pair with $M_1 = M_2 = 1.37M_\odot$ [25, 26]. The pure-neutron or hybrid stars with such mass in the list are S1, S2, S7, S10, S13, T1, T2 and T11. In this set, unlike S13 and T11 which belong to the third scenario, the other stars belong to the first two scenarios and have none or little dark matter.

Since $\tilde{\Lambda} = (\Lambda_1 + \Lambda_2)/2$ for the equal-mass binary, any two stars from the same type labelled by either **a**, **b** or **c**, e.g. two S2's, two S13's, {S1, S2}, {T1, T2}, or {S10, S13}, etc, can form a binary of hybrid stars with $\tilde{\Lambda}$ close to it observational upper bound to explain GW170817.

In contrast, for GW190425 the inferred total mass $M_1 + M_2 \simeq 3.4_{-0.1}^{+0.3} M_\odot$, with $M_1 \in (1.62, 1.88)M_\odot$, $M_2 \in (1.45, 1.69)M_\odot$ and $\tilde{\Lambda} \leq 600$ for low spin prior, or with $M_1 \in (1.61, 2.52)M_\odot$, $M_2 \in (1.12, 1.68)M_\odot$ and $\tilde{\Lambda} \leq 1100$ for high-spin prior [27]. From the Table 1, we can find the following five pairs of hybrid stars with Holo EoS to explain GW190425: (1) {S3, S5} with $\tilde{\Lambda} = 771$, (2) two S4's with $\tilde{\Lambda} = 593$, (3) two S8's with $\tilde{\Lambda} = 220$, (4) two S11's with $\tilde{\Lambda} = 260$, (4) two S12's with $\tilde{\Lambda} = 76$ and (5) two S14's with $\tilde{\Lambda} = 38$. For the SLy4 case, we also have

Index	Type	M	M_D/M	R	R_D	R_N	Λ
S1	aRD	1.37	0	13.11	0		709
S2	aRD	1.37	0.05	13.71	4.5		1068
S3	aRD	2.01	0.32	13.41	8		83
S4	aRD	1.7	0.19	14.86	8		593
S5	aRD	1.4	0.15	15.5	8		2688
S6	aRD	3.42	0.91	26.4	25		213
S7	cRD	1.37	0.09	12.6	4.5		598
S8	aRN	1.7	0.12	18.09		10.7	220
S9	aRN	3.5	1.0	33.34		0	390
S10	bRD	1.37	0.06	13.44	4.5		893
S11	bRD	1.7	0.36	13.59	8		260
S12	bRN	1.7	0.05	13.22		10.7	76
S13	bMX	1.34	0.27	10.26	10.26	10.23	125
S14	bMX	1.7	0.01	10.98	5.07	10.98	38
T1	aRD	1.37	0	11.59	0		360
T2	aRD	1.37	0.07	11.96	4.5		486
T3	aRD	1.9	0.65	10.77	8		21
T4	aRD	1.7	0.26	13.19	8		352
T5	aRD	1.5	0.21	13.54	8		999
T6	aRD	3.42	0.93	26.91	25		1802
T7	aRN	1.7	0.15	12.90		10.7	79
T8	aRN	3.5	1.0	33.34		0	390
T9	bRD	1.7	0.53	11.63	8		104
T10	bRN	1.7	0.01	11.97		10.7	77
T11	bMX	1.37	0.30	10.14	10.14	9.35	87
T12	bMX	1.7	0.11	10.06	7.62	10.06	25

Table 1. List of 26 specific hybrid stars, most of which are indicated on Fig. 5, 7, 9 and 10. The first entry labels the stars, and the second entry is the type of hybrid stars as defined earlier, then the subsequent entries are total mass, mass ratio of dark matter to the total mass, total radius, respective core radius and TLN. The core pressures of dark matter for S13, S14, T11 and T12 are $4.7 \times 10^{-4} p_\odot$, $2.8 \times 10^{-5} p_\odot$, $2.5 \times 10^{-4} p_\odot$ and $2.0 \times 10^{-4} p_\odot$, respectively. Note the S7 hybrid star is for $\mathcal{A} = 0.341$ and $\mathcal{B} = 0.055$ (labelled as **cRD**). Also S9 and T8 actually refer to the same pure dark star.

(1) two T4's with $\tilde{\Lambda} = 352$, (2) {T3, T5} with $\tilde{\Lambda} = 348$, (3) two T7's with $\tilde{\Lambda} = 79$, (4) two T9's with $\tilde{\Lambda} = 104$, (5) two T10's with $\tilde{\Lambda} = 77$ and (6) two T12's with $\tilde{\Lambda} = 25$. From Table 1 it is interesting to see that the values of Λ cover a wide range, even with the same masses.

6 Parameter estimation for EoS of dark matter

Finally, we can use the data of GW190425 and its parameter estimation result given in [27] to further map out the posteriors for the EoS parameter $\mathcal{B} \sim \frac{0.08}{\sqrt{\Lambda}} \left(\frac{m}{\text{GeV}}\right)^2$ and the core radius r_W for the first two scenarios by fixing $\mathcal{A} = 0.305$ of Holo EoS. We do not intend to be complete for considering all the scenarios and possible EoS in this study, but just show an example for the cases chosen above to elaborate the procedure for the future systematic studies of more GW data.

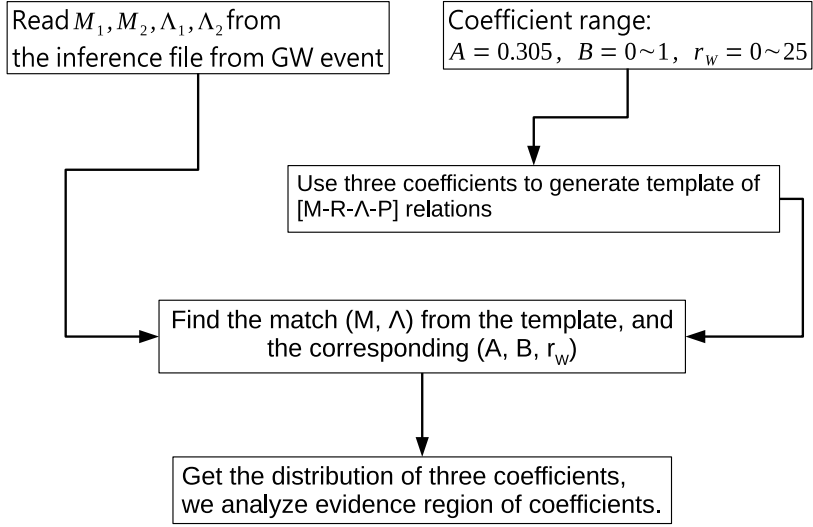


Figure 12. Flow chart of obtaining the posteriors of hybrid stars' properties from the posteriors of GW events for a possible binary hybrid-star candidate such as GW190425. See the main text for more detailed explanation.

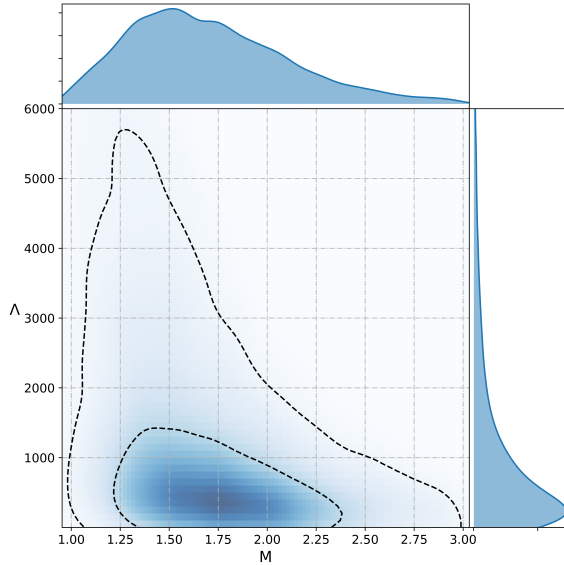


Figure 13. The joint posteriors for M and Λ of the GW190425 obtained from the inference file of the Gravitational Wave Open Science Center (GWOSC) [48]. The contour lines are represented as the credible interval of 50% and 90%.

The key procedure of the parameter estimation goes as follows: (1) obtaining the sample bank of the posteriors for $M_{1,2}$ and $\Lambda_{1,2}$ from [27]; (2) obtaining the bank of $M_{1,2}$ and $\Lambda_{1,2}$ from solving TOV and the evaluating TLNs by finely tuning \mathcal{B} and r_w with fixed $\mathcal{A} = 0.305$; (3) matching the bank of (1) to the bank of (2) to obtain the sample bank of \mathcal{B} and r_w and thus their posteriors. The flow chart for the above procedure of the mapping the posteriors

of GW190425 to the posteriors of hybrid star properties is shown in Fig. 12.

Some details of the flow goes as follows. We have three adjustable coefficients of the hybrid star, \mathcal{A} , \mathcal{B} and r_W . Their ranges are chosen as follows: $\mathcal{A} = 0.305$, $\mathcal{B} = [0, 3]$ and $r_W = [0, 25]$. Within these parameter ranges, we then generate the corresponding sample bank labelled by $[M, R, \Lambda, P, \mathcal{A}, \mathcal{B}$ and $r_W]$ by making the samples as uniform as possible. At the same time, we also get the sample bank labelled by $[M_1, M_2, \Lambda_1, \Lambda_2]$ from the inference file of Gravitational Wave Open Science Center (GWOSC) for the event GW190425, which is shown in Fig. 13. We then perform the full search to match these two sample banks. In the mean time we also perform the 3D surface interpolation to make up the insufficient coverup of discrete data set.

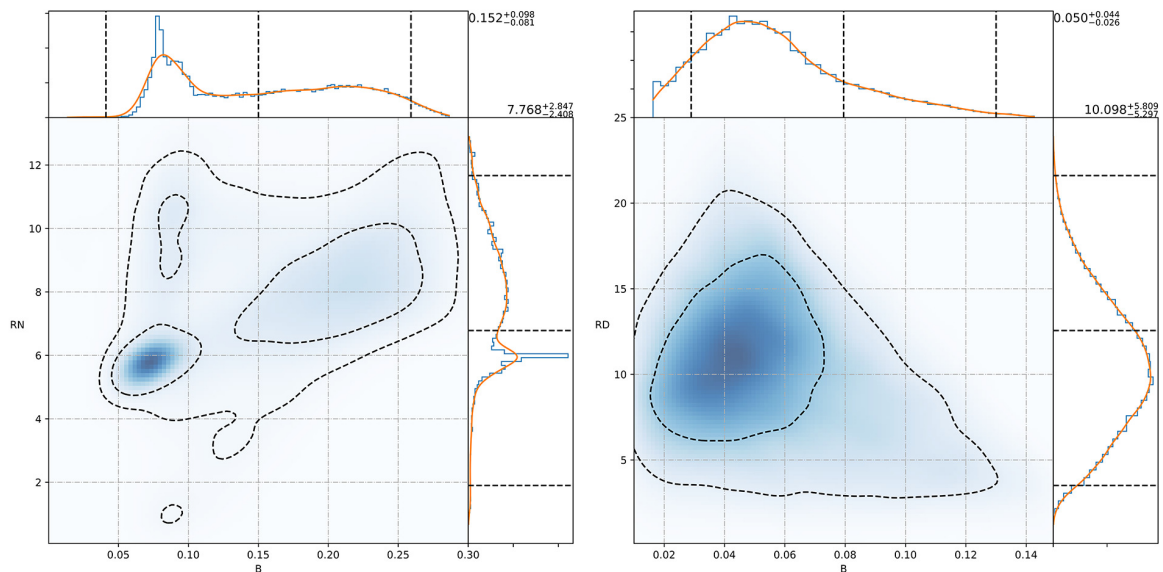


Figure 14. Posteriors for the EoS parameter \mathcal{B} (horizontal axis) of the SIDM and the core-radius r_W (vertical axis) for the first (left sub-figure) and the second (right sub-figure) scenarios by fixing $\mathcal{A} = 0.305$. The inner circled regions are 50% credible interval, and the outer ones are 90% credible interval. The inferred best-fitted values of \mathcal{B} and r_W are given in the main text.

The results are shown in Fig. 14. The inferred best-fitted values are, for the first scenario $\mathcal{B} = 0.152^{+0.098}_{-0.081}$ and $\mathbf{RN} = 7.768^{+2.847}_{-2.408}$ km, for the second scenario $\mathcal{B} = 0.050^{+0.044}_{-0.026}$ and $\mathbf{RD} = 10.098^{+5.809}_{-5.297}$ km. Together with the astrophysical constraint (2.2), we can infer the parameters of SIDM and obtain $\lambda \in (200, 5255)$ and $m \in (3.54, 15.05)$ GeV for the first scenario, and $\lambda \in (54, 1625)$ and $m \in (1.49, 6.88)$ GeV for the second scenario. Both satisfy well the constraint $\lambda M_{\text{planck}}^2/m^2 \gg 1$. Further GW data is expected to sharpen the above estimation. A full-scale study of the posteriors for \mathcal{A} , \mathcal{B} and r_W for all three hybrid-star scenarios to infer the parameters m and λ of SIDM by using more GW data and the other astrophysical constraints on SIDM will be given in a future work.

7 Conclusion

Dark matter has an abundance much higher than that of normal matter, though the self-interaction of dark matter is considered to be weak, we cannot exclude the possibility for it to form compact objects like dark stars. The lack of traditional astronomical observations of dark

stars on the contrary indicates the importance of GW events as probes for them. Therefore, we examine the GW properties of dark or hybrid stars by assuming their existence, rather than ruling them out for granted. We choose some special EoSs for neutrons and dark bosons in this paper, but the method we develop here can be applied to any EoS. That means, any compact star with two or more components can be discussed using our model (One needs to pay extra attention to the dynamical relations if the components can change to each other at different phases, as for the case of quark stars.).

In this paper we have shown that our hybrid-star scenarios can well explain the observed GW170817 and GW190425 which are usually considered as binary neutron stars. We expect the coming CBC data of LIGO/Virgo's O3 will shed more light on our approach to the hybrid stars and the associated dark matter model. Our study integrates three areas: gravitational waves, astronomy and particle physics. The vision becomes more clear than confined in a single subject. By combining knowledge from different perspectives, our discussion reveals the possibility that a hybrid star might be heavier than it appears, with a visible neutron core and an invisible dark crust. This not only is consistent with GW170817 and the 2 solar mass constraint, but also could explain both the large masses and relatively big tidal deformability of GW190425. We examine systematically the multi-component TOV equations and tidal deformability, which are not widely discussed before. In our first two scenarios, the junction condition for altering the components is taken into steady deliberation. In our scenario three, we evaluate the tidal deformability for multi-component stars for the first time in the literature.

An important feature of the hybrid stars from our results is that they in general span a wider mass and TLN range than their pure neutron or dark stars counterparts of a given EoS. Although this is expected due to the introduction of an additional component, this feature will help to distinguish them from their pure cousins in the data analysis of the GW observational data. Of course, the distinguishability will be limited by the uncertainty of the dark matter EoS and the amount of dark matter inside the hybrid stars. However, we can expect this kind of systematic uncertainty will be lifted once the quality and amount of the GW data are improved in the coming future observations. Especially, if one observes the compact stars with wider range of masses and TLNs with enough accuracy, then our scenarios of hybrid stars will be justified. For example, the third scenario admits more compact hybrid stars than the neutron stars of a given EoS, thus yields lower TLNs. Similarly, the first two scenarios in general yield less compact stars than the pure neutron stars, and thus higher TLNs. These will then serve as the guideline when searching the hybrid stars for the future observations with higher accuracy in measuring TLNs.

For the future work, We will make the parameter estimation more clear, and consider more models for dark matters. For the EoS of dark boson, we choose a toy model of SIDM with ϕ^4 potential for simplicity. In the future, we will discuss more general models with higher ϕ corrections. Through our analysis, the coupling constant λ can be induced from GW events, thus confine the dark matter models. Another interesting direction is to discuss the process of how to form dark or hybrid stars. As mentioned before, The self-interaction cross section of dark matter could be dramatically magnified by forming dark matter nuggets. Or dark matters can accumulate gravitationally through the Bondi accretion. We will follow those lines and explore further possibilities.

Acknowledgement

FLL and GZH are supported by Taiwan Ministry of Science and Technology (MoST) through Grant No. 106-2112-M-003-004-MY3. KZ (Hong Zhang) is supported by MoST through Grant No. 107-2811-M-003-511. We thank Yen-Hsun Lin, Alessandro Parisi and other TGWG members for helpful discussions. We also thank NCTS for partial financial support.

A Unify TOV equations and Tidal force for multi-component cases

The metric of a spherical, static star can be given as

$$ds_0^2 = g_{\alpha\beta}^{(0)} dx^\alpha dx^\beta = -e^{2\phi(r)} dt^2 + e^{\lambda(r)} dr^2 + r^2 (d\theta^2 + \sin^2 \theta d\psi^2), \quad (\text{A.1})$$

where $e^{\phi(r)}$ is the lapse function with $\phi(r)$ the metric potential, and $e^{\lambda(r)} = (1 - \frac{2G_N m(r)}{rc^2})^{-1}$ with $m(r)$ the gravitational mass inside radius r . The Tolman-Oppenheimer-Volkoff (TOV) equations [49] can be obtained from Einstein equations $\frac{8\pi G_N}{c^4} T_{\mu\nu} = G_{\mu\nu}$, by noticing that the stress-energy tensor is diagonal for perfect fluid, $T_0^0 = \rho c^2$ and $T_i^j = -p\delta_i^j$.

The TOV equations for multi-component cases read [50, 51]

$$\begin{aligned} \frac{dp_I}{dr} &= -G_N(\rho_I + p_I/c^2) \frac{m + 4\pi r^3 p/c^2}{r(r - 2G_N m/c^2)}, \\ \frac{dm_I}{dr} &= 4\pi r^2 \rho_I, \\ \frac{d\phi}{dr} &= \frac{m + 4\pi r^3 p/c^2}{r(r - 2G_N m/c^2)}. \end{aligned} \quad (\text{A.2})$$

Here $m = \sum_I m_I$ and $p = \sum_I p_I$ by summing the contributions from different fluids marked by the subscript I . For the cases discussed in this paper, $I = D$ or N , standing for dark boson or neutron.

For convenience, we chose to express all the physical quantities in $G_N = c = 1$ convention. Given the relation between ρ_I and p_I , i.e., the EoS, one can solve the TOV equation for a star with a certain initial central pressure. The boundary condition $p(r = R) = 0$ defines the radius R of the compact star, and $m(R)$ gives its total mass. For the first two scenarios, we just divide the equations by two parts at the core radius r_W . Each part behaves like a single-component case, but with the pressure p continuous at the junction position r_W . For the third scenario, we need initial pressures for both p_D and p_N . One important fact to realize for this scenario is that, the individual p_I do not necessarily fall to zero simultaneously. When one p_I reaches zero, we set it to zero from that on, read off the current radius r_W , and continue to solve the equations until the total radius R , where the other p_I goes zero.

Once we solve a stable compact star configuration, we can study its tidal deformability. In [46] it shows that when considering a static, spherically symmetric star of mass M under an external quadrupolar field \mathcal{E}_{ij} , it will response a quadrupole moment Q_{ij} ,

$$Q_{ij} = - \left(\frac{M}{M_\odot} \right)^5 \Lambda \mathcal{E}_{ij}. \quad (\text{A.3})$$

Here the constant Λ is related to the $l = 2$ tidal Love number k_2 by

$$\Lambda = \frac{2}{3} k_2 C^{-5}, \quad (\text{A.4})$$

where $C = M/R$ is the "compactness" of the star.

The calculation of k_2 goes as follows. The spacetime metric is

$$g_{\alpha\beta} = g_{\alpha\beta}^{(0)} + h_{\alpha\beta}, \quad (\text{A.5})$$

with $h_{\alpha\beta}$ a linearized perturbation. When restricting to the $l = 2$, static, even-parity perturbations in the Regge-Wheeler gauge, it reads

$$h_{\alpha\beta} = \text{diag} \left[e^{-\nu(r)} H_0(r), e^{\lambda(r)} H_2(r), r^2 K(r), r^2 \sin^2 \theta K(r) \right] Y_{2m}(\theta, \varphi), \quad (\text{A.6})$$

with $\nu(r) = 2\phi(r)$. After some analysis it follows that $H_2 = H_0 \equiv H$, which is the solution of the equation

$$H''(r) + H'(r) \left[\frac{2}{r} + e^{\lambda(r)} \left(\frac{2m(r)}{r^2} + 4\pi r(p(r) - \rho(r)) \right) \right] + H(r)Q(r) = 0, \quad (\text{A.7})$$

where the primes denote derivatives with respect to r , and

$$Q(r) = 4\pi e^{\lambda(r)} \left(5\rho(r) + 9p(r) + \frac{\rho(r) + p(r)}{c_s^2(r)} \right) - 6 \frac{e^{\lambda(r)}}{r^2} - (\nu'(r))^2. \quad (\text{A.8})$$

For multi-component cases, the discussion is the same, just with Q replaced by (3.6).

(A.7) is a second order differential equation of H , but to get k_2 we only need a combination $y(r) = rH'(r)/H(r)$. In [47] the calculation is simplified by rewriting (A.7) as a first-order differential equation of $y(r)$:

$$ry'(r) + y(r)^2 + y(r)e^{\lambda(r)} [1 + 4\pi r^2(p(r) - \rho(r))] + r^2 Q(r) = 0. \quad (\text{A.9})$$

We can then solve it numerically with the initial condition $y(0) = 2$, and the Love number k_2 is given in terms of the compactness C and the quantity $y_R \equiv y(R)$ as following:

$$k_2 = \frac{8C^5}{5} (1 - 2C)^2 [2 + 2C(y_R - 1) - y_R] \times \left\{ 2C(6 - 3y_R + 3C(5y_R - 8)) + 4C^3 [13 - 11y_R + C(3y_R - 2) + 2C^2(1 + y_R)] + 3(1 - 2C)^2 [2 - y_R + 2C(y_R - 1)] \log(1 - 2C) \right\}^{-1}. \quad (\text{A.10})$$

A.1 Junction condition between core and crust

When we consider a hybrid star with two layers of different components, the TOV and tidal equations need be solved separately and connect with correct boundary conditions. The pressure p is continuous, energy density ρ is uncountinuous, and the y encounters a jump, which need be taken care of. More details can be found in [47].

Suppose at radius r_W one component is changed to another, where the pressure reads p_W . The sound speed in the vicinity of a density discontinuity is

$$\frac{d\rho}{dp} = \frac{1}{c_s^2} = \frac{d\rho}{dp} \Big|_{p \neq p_W} + \Delta\rho_p \delta(p - p_W), \quad (\text{A.11})$$

where $\Delta\rho_p = \rho(p_W + 0) - \rho(p_W - 0)$ is the energy density jump across p_W . Yet since p decreases as r increases, equivalently $\Delta\rho_p = -(\rho(r_W + 0) - \rho(r_W - 0)) \equiv -\Delta\rho_r$.

When we integrate (A.9) in an infinitely small region around the junction radius r_W , most of the terms give 0, and only the terms proportional to δ functions can contribute. Therefore, at the position r_W ,

$$ry'(r)|_{r=r_W} + r^2 4\pi e^{\lambda(r)} (\rho(r) + p(r)) \frac{d\rho}{dp}|_{r=r_W} = 0. \quad (\text{A.12})$$

Since $\frac{d\rho}{dp} = \frac{d\rho}{dr} \frac{1}{dp/dr}$, where dp/dr can be read off from the first TOV equation (A.2), and $\frac{d\rho}{dr}|_{r=r_W} = \Delta\rho_r \delta(r - r_W)$, we obtain that

$$y(r_W + \epsilon) = y(r_W - \epsilon) + \frac{\rho(r_W + \epsilon) - \rho(r_W - \epsilon)}{p + m(r_W)/(4\pi r_W^3)}, \quad (\text{A.13})$$

with $\epsilon \rightarrow 0$. As a result, we can solve the TOV and tidal deformation equations by two steps connected at r_W , with the pressure p continuous, and y changes as above.

References

- [1] M. Klasen, M. Pohl and G. Sigl, “Indirect and direct search for dark matter,” *Prog. Part. Nucl. Phys.* **85**, 1 (2015). [arXiv:1507.03800 [hep-ph]].
- [2] E. Aprile *et al.* [XENON Collaboration], “First Dark Matter Search Results from the XENON1T Experiment,” *Phys. Rev. Lett.* **119**, no. 18, 181301 (2017). [arXiv:1705.06655 [astro-ph.CO]].
- [3] X. Cui *et al.* [PandaX-II Collaboration], “Dark Matter Results From 54-Ton-Day Exposure of PandaX-II Experiment,” *Phys. Rev. Lett.* **119**, no. 18, 181302 (2017). [arXiv:1708.06917 [astro-ph.CO]].
- [4] D. S. Akerib *et al.* [LUX Collaboration], “Results from a search for dark matter in the complete LUX exposure,” *Phys. Rev. Lett.* **118**, no. 2, 021303 (2017). [arXiv:1608.07648 [astro-ph.CO]].
- [5] C. Kouvaris and N. G. Nielsen, “Asymmetric Dark Matter Stars,” *Phys. Rev. D* **92**, no.6, 063526 (2015) doi:10.1103/PhysRevD.92.063526 [arXiv:1507.00959 [hep-ph]].
- [6] A. Maselli, P. Pnigouras, N. G. Nielsen, C. Kouvaris and K. D. Kokkotas, “Dark stars: gravitational and electromagnetic observables,” *Phys. Rev. D* **96**, no. 2, 023005 (2017). [arXiv:1704.07286 [astro-ph.HE]].
- [7] N. Sennett, T. Hinderer, J. Steinhoff, A. Buonanno and S. Ossokine, “Distinguishing Boson Stars from Black Holes and Neutron Stars from Tidal Interactions in Inspiring Binary Systems,” *Phys. Rev. D* **96**, no. 2, 024002 (2017). [arXiv:1704.08651 [gr-qc]].
- [8] G. Jungman, M. Kamionkowski and K. Griest, “Supersymmetric dark matter,” *Phys. Rept.* **267**, 195 (1996). [hep-ph/9506380].
- [9] D. N. Spergel and P. J. Steinhardt, “Observational evidence for selfinteracting cold dark matter,” *Phys. Rev. Lett.* **84**, 3760 (2000). [astro-ph/9909386].
- [10] M. Rocha, A. H. G. Peter, J. S. Bullock, M. Kaplinghat, S. Garrison-Kimmel, J. Onorbe and L. A. Moustakas, “Cosmological Simulations with Self-Interacting Dark Matter I: Constant Density Cores and Substructure,” *Mon. Not. Roy. Astron. Soc.* **430**, 81 (2013). [arXiv:1208.3025 [astro-ph.CO]].
- [11] A. H. G. Peter, M. Rocha, J. S. Bullock and M. Kaplinghat, “Cosmological Simulations with Self-Interacting Dark Matter II: Halo Shapes vs. Observations,” *Mon. Not. Roy. Astron. Soc.* **430**, 105 (2013). [arXiv:1208.3026 [astro-ph.CO]].

- [12] M. Kaplinghat, S. Tulin and H. B. Yu, “Dark Matter Halos as Particle Colliders: Unified Solution to Small-Scale Structure Puzzles from Dwarfs to Clusters,” *Phys. Rev. Lett.* **116**, no. 4, 041302 (2016). [arXiv:1508.03339 [astro-ph.CO]].
- [13] M. Colpi, S. L. Shapiro and I. Wasserman, “Boson Stars: Gravitational Equilibria of Selfinteracting Scalar Fields,” *Phys. Rev. Lett.* **57**, 2485 (1986).
- [14] F. E. Schunck and E. W. Mielke, “General relativistic boson stars,” *Class. Quant. Grav.* **20**, R301 (2003). [arXiv:0801.0307 [astro-ph]].
- [15] J. Eby, C. Kouvaris, N. G. Nielsen and L. Wijewardhana, “Boson Stars from Self-Interacting Dark Matter,” *JHEP* **02**, 028 (2016) doi:10.1007/JHEP02(2016)028 [arXiv:1511.04474 [hep-ph]].
- [16] M. Deliyergiyev, A. Del Popolo, L. Tolos, M. Le Delliou, X. Lee and F. Burgio, “Dark compact objects: an extensive overview,” *Phys. Rev. D* **99**, no. 6, 063015 (2019). [arXiv:1903.01183 [gr-qc]].
- [17] G. Battaglia *et al.*, “The Radial velocity dispersion profile of the Galactic Halo: Constraining the density profile of the dark halo of the Milky Way,” *Mon. Not. Roy. Astron. Soc.* **364**, 433 (2005); Erratum: [*Mon. Not. Roy. Astron. Soc.* **370**, 1055 (2006)]. [astro-ph/0506102].
- [18] C. Kouvaris and P. Tinyakov, “Constraining Asymmetric Dark Matter through observations of compact stars,” *Phys. Rev. D* **83**, 083512 (2011) [arXiv:1012.2039 [astro-ph.HE]].
- [19] S. D. McDermott, H. B. Yu and K. M. Zurek, “Constraints on Scalar Asymmetric Dark Matter from Black Hole Formation in Neutron Stars,” *Phys. Rev. D* **85**, 023519 (2012) [arXiv:1103.5472 [hep-ph]].
- [20] M. I. Gresham, H. K. Lou and K. M. Zurek, “Nuclear Structure of Bound States of Asymmetric Dark Matter,” *Phys. Rev. D* **96**, no. 9, 096012 (2017) doi:10.1103/PhysRevD.96.096012 [arXiv:1707.02313 [hep-ph]].
- [21] M. I. Gresham, H. K. Lou and K. M. Zurek, “Early Universe synthesis of asymmetric dark matter nuggets,” *Phys. Rev. D* **97**, no. 3, 036003 (2018) doi:10.1103/PhysRevD.97.036003 [arXiv:1707.02316 [hep-ph]].
- [22] M. I. Gresham, H. K. Lou and K. M. Zurek, “Astrophysical Signatures of Asymmetric Dark Matter Bound States,” *Phys. Rev. D* **98**, no. 9, 096001 (2018) doi:10.1103/PhysRevD.98.096001 [arXiv:1805.04512 [hep-ph]].
- [23] A. Coskuner, D. M. Grabowska, S. Knapen and K. M. Zurek, “Direct Detection of Bound States of Asymmetric Dark Matter,” *Phys. Rev. D* **100**, no. 3, 035025 (2019) doi:10.1103/PhysRevD.100.035025 [arXiv:1812.07573 [hep-ph]].
- [24] R. G. Edgar, “A Review of Bondi-Hoyle-Lyttleton accretion,” *New Astron. Rev.* **48**, 843 (2004) doi:10.1016/j.newar.2004.06.001 [astro-ph/0406166].
- [25] B. P. Abbott *et al.* [LIGO Scientific and Virgo Collaborations], “GW170817: Observation of Gravitational Waves from a Binary Neutron Star Inspiral,” *Phys. Rev. Lett.* **119**, no. 16, 161101 (2017). [arXiv:1710.05832 [gr-qc]].
- [26] B. P. Abbott *et al.* [LIGO Scientific and Virgo Collaborations], “Properties of the binary neutron star merger GW170817,” *Phys. Rev. X* **9**, no. 1, 011001 (2019). [arXiv:1805.11579 [gr-qc]].
- [27] B. P. Abbott *et al.* [LIGO Scientific and Virgo Collaborations], “GW190425: Observation of a Compact Binary Coalescence with Total Mass $\sim 3.4M_{\odot}$,” arXiv:2001.01761 [astro-ph.HE].
- [28] M. Kuster, G. Raffelt and B. Beltran, “Axions: Theory, cosmology, and experimental searches. Proceedings, 1st Joint ILIAS-CERN-CAST axion training, Geneva, Switzerland, November 30-December 2, 2005,” *Lect. Notes Phys.* **741**, pp.1-258 (2008)

- [29] J. Eby, M. Leembruggen, L. Street, P. Suranyi and L. R. Wijewardhana, “Global view of QCD axion stars,” *Phys. Rev. D* **100**, no.6, 063002 (2019) doi:10.1103/PhysRevD.100.063002 [arXiv:1905.00981 [hep-ph]].
- [30] O. A. Hannuksela, K. W. Wong, R. Brito, E. Berti and T. G. Li, “Probing the existence of ultralight bosons with a single gravitational-wave measurement,” *Nature Astron.* **3**, no.5, 447-451 (2019) doi:10.1038/s41550-019-0712-4 [arXiv:1804.09659 [astro-ph.HE]].
- [31] C. Hoyos, D. Rodriguez Fernandez, N. Jokela and A. Vuorinen, “Holographic quark matter and neutron stars,” *Phys. Rev. Lett.* **117**, no. 3, 032501 (2016). [arXiv:1603.02943 [hep-ph]].
- [32] E. Annala, C. Ecker, C. Hoyos, N. Jokela, D. Rodriguez Fernandez and A. Vuorinen, “Holographic compact stars meet gravitational wave constraints,” *JHEP* **1812**, 078 (2018). [arXiv:1711.06244 [astro-ph.HE]].
- [33] F.-L. Lin, K. Zhang, unpublished work.
- [34] F. Douchin and P. Haensel, “A unified equation of state of dense matter and neutron star structure,” *Astron. Astrophys.* **380**, 151 (2001) doi:10.1051/0004-6361:20011402 [arXiv:astro-ph/0111092 [astro-ph]].
- [35] <https://compose.obspm.fr/eos/134/>
- [36] K. Zhang, T. Hirayama, L. W. Luo and F. L. Lin, “Compact Star of Holographic Nuclear Matter and GW170817,” *Phys. Lett. B* **801**, 135176 (2020). [arXiv:1902.08477 [hep-ph]].
- [37] T. Sakai and S. Sugimoto, “Low energy hadron physics in holographic QCD,” *Prog. Theor. Phys.* **113**, 843 (2005). [hep-th/0412141].
- [38] T. Sakai and S. Sugimoto, “More on a holographic dual of QCD,” *Prog. Theor. Phys.* **114**, 1083 (2005). [hep-th/0507073].
- [39] H. Hata, T. Sakai, S. Sugimoto and S. Yamato, “Baryons from instantons in holographic QCD,” *Prog. Theor. Phys.* **117**, 1157 (2007). [hep-th/0701280 [HEP-TH]].
- [40] J. M. Lattimer, “The nuclear equation of state and neutron star masses,” *Ann. Rev. Nucl. Part. Sci.* **62** (2012) 485. [arXiv:1305.3510 [nucl-th]].
- [41] J. M. Bardeen, K. S. Thorne and D. W. Meltzer, “A Catalogue of Methods for Studying the Normal Modes of Radial Pulsation of General-Relativistic Stellar Models,” *Astrophys. J.* **145**, 109 (1966).
- [42] M. G. Alford, S. P. Harris and P. S. Sachdeva, “On the stability of strange dwarf hybrid stars,” *Astrophys. J.* **847**, no.2, 109 (2017) doi:10.3847/1538-4357/aa8509 [arXiv:1705.09880 [astro-ph.HE]].
- [43] J. M. Lattimer and A. W. Steiner, “Neutron Star Masses and Radii from Quiescent Low-Mass X-ray Binaries,” *Astrophys. J.* **784**, 123 (2014) [arXiv:1305.3242 [astro-ph.HE]].
- [44] E. M. Cackett, J. M. Miller, S. Bhattacharyya, J. E. Grindlay, J. Homan, M. van der Klis, T. E. Strohmayer and R. Wijnands, “Relativistic iron emission lines in neutron star low-mass X-ray binaries as probes of neutron star radii,” *Astrophys. J.* **674**, 415 (2008) [arXiv:0708.3615 [astro-ph]].
- [45] F. Ozel, D. Psaltis, T. Guver, G. Baym, C. Heinke and S. Guillot, “The Dense Matter Equation of State from Neutron Star Radius and Mass Measurements,” *Astrophys. J.* **820**, no. 1, 28 (2016) [arXiv:1505.05155 [astro-ph.HE]].
- [46] T. Hinderer, “Tidal Love numbers of neutron stars,” *Astrophys. J.* **677**, 1216 (2008). [arXiv:0711.2420 [astro-ph]].
- [47] S. Postnikov, M. Prakash and J. M. Lattimer, “Tidal Love Numbers of Neutron and Self-Bound Quark Stars,” *Phys. Rev. D* **82**, 024016 (2010). [arXiv:1004.5098 [astro-ph.SR]].

- [48] M. Vallisneri, J. Kanner, R. Williams, A. Weinstein and B. Stephens, “The LIGO Open Science Center,” J. Phys. Conf. Ser. **610**, no. 1, 012021 (2015) doi:10.1088/1742-6596/610/1/012021 [arXiv:1410.4839 [gr-qc]].
- [49] Christian D. Ott, *Static Spherically-Symmetric Stellar Structure in General Relativity*, 2013.
- [50] S. Mukhopadhyay, D. Atta, K. Imam, D. N. Basu and C. Samanta, “Compact bifluid hybrid stars: Hadronic Matter mixed with self-interacting fermionic Asymmetric Dark Matter,” Eur. Phys. J. C **77**, no. 7, 440 (2017) Erratum: [Eur. Phys. J. C **77**, no. 8, 553 (2017)] doi:10.1140/epjc/s10052-017-5006-3, 10.1140/epjc/s10052-017-5070-8 [arXiv:1612.07093 [nucl-th]].
- [51] Z. Rezaei, “Double dark-matter admixed neutron star,” Int. J. Mod. Phys. D **27**, no. 16, 1950002 (2018) doi:10.1142/S0218271819500020 [arXiv:1807.01781 [astro-ph.HE]].